Towards Correlated Photon Triplets from Six-Wave Mixing

Ng Boon Long

A thesis submitted in partial fulfillment of the requirements for the degree of Bachelor of Science with Honours

Supervisor: Professor Christian Kurtsiefer

Department of Physics

National University of Singapore

2017/2018

Contents

Acknowledgement

I hereby express my greatest gratitude to my supervisor, Professor Christian Kurtsiefer for the guidance and opportunity to work on such an interesting project. It has been an amazing year and wonderful experience to work in this group.

To my mentor Mathias, I appreciate that he has been extremely patient in mentoring. He carefully guided me from time to time, starting from basic explanation in detail, to giving me the courage to try and learn from error. Without his support and encouragement, chances that I cannot achieve so many things in this project. I would also like to express my gratitude to Alessandro for his encouragement and guidance.

To Janet and Wilson, your kindness and laughter has made the project a much more relax work to do. My sincere thanks to all other members of Quantum Optics group, it has been a great time working with them.

Chapter 1

Introduction

Time-correlated photon pairs have been a useful resource for quantum communication protocols[1, 2] and quantum optics experiments such as single atom light interaction[3, 4, 5, 6] and quantum memory[7]. These photon pairs are also used as sources of heralded single photons. By using the time correlation of the generated photon pairs, the detection of one photon of the pair guarantees the presence of its twin.

Time-correlated photon pairs can be generated via the parametric processes such as spontaneous parametric down-conversion (SPDC) in non-central-symmetric medium[8], four-wave mixing in atomic medium[9] and optical fibres[10, 11]. In a parametric process, the state of the medium remains unchanged before and after the process. This implies that the energy and momentum are conserved for the light fields involved in the process.

When a non-linear dielectric material is placed within an external optical field, the field induces a dipole moment and polarises the material. The response of a dielectric material to the applied optical field can be written as series expansion[12]

$$P = \epsilon_0(\chi^{(1)}E + \chi^{(2)}E^2 + \chi^{(3)}E^3 + ...) \tag{1.1}$$

where E is the amplitude of applied optical field, P is the dipole moment per unit volume, also known as polarization of the material. $\chi^{(1)}$ is the linear susceptibility that related to refractive index of the medium by $n = \sqrt{1 + \chi^{(1)}}$ while $\chi^{(n)}$ is the n-th order non-linear susceptibility of the medium. Usually the higher order terms are very small and the non-linear effects are negligible. However, for specific materials and sufficiently high field strengths, these terms become significant and noticeable.

SPDC in nonlinear crystals make use of the $\chi^{(2)}$ effect of non-linear crystal to create the photon pairs from a single pump beam. For the past three decades, this parametric process has been the workhorse because of its robustness in generating photon pairs that have well defined spatial modes. However, the photon pairs generated from SPDC have very wide optical bandwidths ranging from 0.1 to 2 THz[8, 13, 14]. The bandwidth of photons generated from SPDC can be narrowed down by some techniques such as optical cavity[15] or time lens[16] but ultimately there will be some trade-off such as decrease in brightness.

We consider a different approach to generate narrowband photon pairs: Four-Wave Mixing (FWM) in cold atomic ensemble[9]. FWM exploits the third order susceptibility, $\chi^{(3)}$ of the atom and has been used to generate correlated photon pairs from non-linear fibre and cold atomic ensembles. Atoms have discrete energy levels which lead to the generation of narrowband photons. Correlated photon pairs generated by FWM in a cold ^{87}Rb atomic ensemble have been observed with an optical bandwidth at the order of 10MHz[9].

In order to study the interaction between light and atoms, photon pairs with a frequency bandwidth that matches the absorption profile of the atoms are expected to have optimal interaction with the atoms. Conventional sources based on down-conversion in nonlinear optical crystals have a bandwidth that is a few orders of magnitude larger than lifetime limited atomic absorption lines, which lowers the probability of photons to interact with atoms. While photon pairs generated by FWM process in an atomic ensemble, have a frequency bandwidth compatible with atomic linewidth, make these photons a suitable candidate in the atom-light experiments[3].

While the generation of correlated photon pairs is well established nowadays, it is natural for us to take one step further to produce photon triplets. Time-correlated photon triplets can be used as heralded photon pairs source and there are a lot of attempts have been done[17, 18, 19, 20]. For example, photon triplets have been generated directly using cascaded photon-pair sources where a single pump beam undergoes SPDC twice[21]. As such, these methods and ideas in generating correlated photon pairs have motivated us in choosing the scheme that we plan to produce photon triplets. In this project, we extend the concept of four-wave mixing to six-wave mixing (SWM) which makes use of the fifth order susceptibility, $\chi^{(5)}$ of the atomic ensembles to generate photon triplets. We expect the generated photon triplets have a narrow bandwidth that is compatible with other atomic systems. To achieve this, we propose a six-wave mixing scheme in Rubidium-87 atomic cloud where we sent in three pump lasers into the atomic cloud and hope to observe time-correlated photon triplets.

1.1 Previous Works: Four Wave Mixing

FWM is a third order non-linear process that involves the interaction of four optical fields in a non-linear medium.

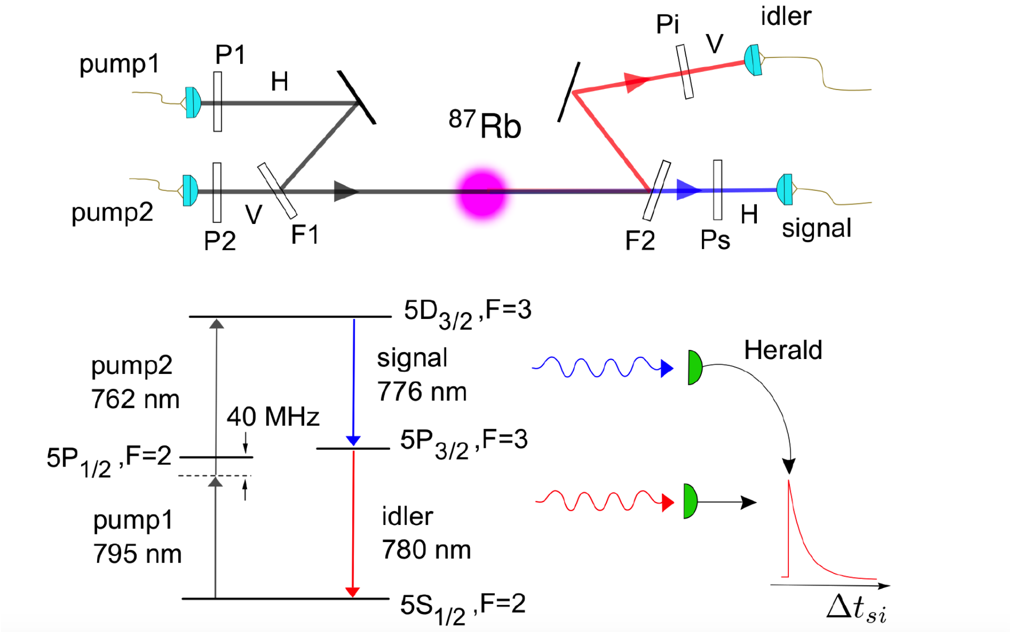

Figure 1.1: (Top) Setup of the FWM process using collinear geometry. The pump beams are combined using an inteference filter (F_1) while the generated photons are then separated by another inteference filter (F_2). (Bottom) Decay scheme of the FWM process.[22] Δt_{si} is the detection time of the idler photon heralded by the signal photon. F_1 and F_2 are interference filter. P_1, P_2, P_i and P_s are polarizer.

Prof Kurtsiefer's group has previously generated narrowband photon pairs via FWM cascade decay scheme in a cloud of cold ^{87}Rb atoms[9]. Pair generation in atoms started by using two pump beams to interact with the atomic cloud and the resulting narrowband time-correlated photon pairs are labelled as signal and idler. The idea of photon heralding is shown in Figure 1.1. The signal photon is used as the herald for the idler photon, which then can be sent to interact with atoms. We can obtain the coherence time of the idler photon by looking at its temporal shape. The frequency bandwidth of this photon is inversely related to its coherence time. In the previous FWM experiment, bandwidth of 24.4±0.1MHZ has been reported[9].

1.1.1 Elongated Magneto-Optical Trap

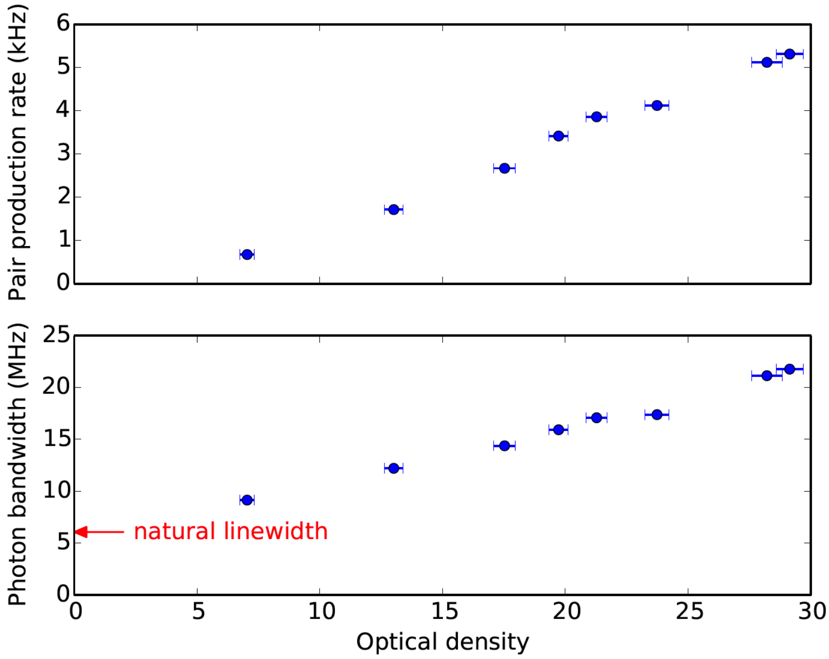

Figure 1.2: The effect of the optical density of cold ^{87}Rb cloud on the photon pair production rate (top) and the bandwidth of the idler photon (bottom)[22]. The red arrow show the natural linewidth of the $5S_{1/2}, F = 2 \rightarrow 5P_{3/2}, F = 3$ transition which is 6.065MHz[23].

The previous work that generates the photon pairs via four-wave mixing cascade decay in a standard Magneto-Optical Trap (MOT) suffers from the pair rate and the bandwidth trade-off[4]. When we want to have more pairs rate with higher optical density (OD), the bandwidth of the photon pair will increase as well. The large bandwidth of the photon decreases the probability of the photon interacting with an atom. There is plenty of literature on the basics of cooling and trapping the atoms in a MOT[24] and is therefore not discussed in more detail.

However, the increasing bandwidth of the idler photon when OD increase[9] might be due to the increase in number of atoms in the cloud with same atomic density, or due to the smaller interatomic spacing because of a denser cloud.

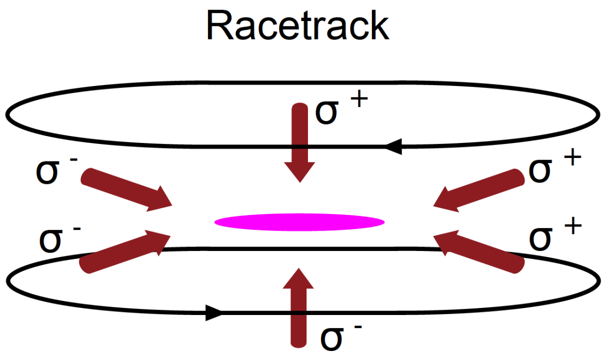

Figure 1.3: Schematic of the elongated MOT using racetrack anti-Helmholtz coils[22].

As such, an elongated MOT[22] had been proposed to investigate the reason for this effect and in turn improve the pair rate and bandwidth trade-off. The elongated MOT can elongate the cloud along one axis by using racetrack shape anti-Helmholtz coils as shown in figure 1.3.

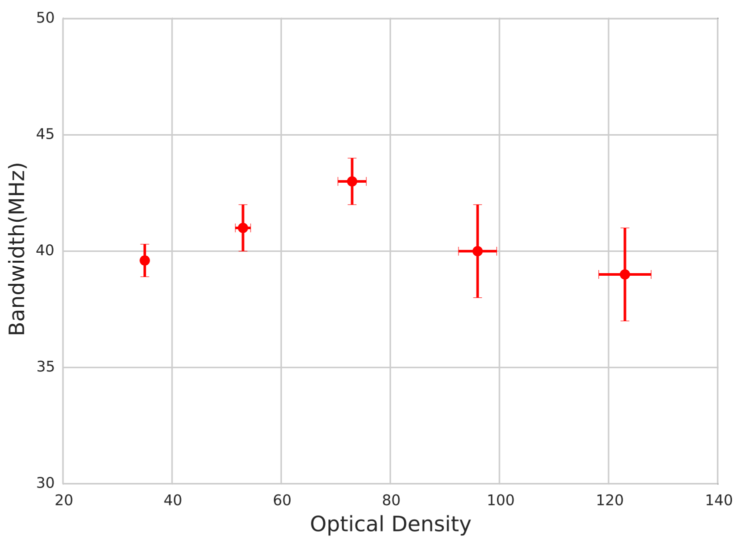

Figure 1.4: Bandwidth of the photon pairs emitted by the elongated cloud of different optical density while the other parameters such as pump power are kept constant. The OD is adjusted by changing the cooling power[25].

The measurement of bandwidth is repeated for several values of OD and we observed something different from expected. From the previous results, the bandwidth of the photon pairs is closely related to the optical density of the cloud. For the spherical MOT of OD range from 5 to 35, the bandwidth of the photon increase linearly from around 10MHz to 25MHz[4, 5]. However for the elongated MOT, the bandwidth of the photon range from 39MHz to 43MHz for optical density higher than 35 and the bandwidth seem to be fairly constant[25]. This means that the bandwidth of the photon pairs that produced by this MOT is saturated at this range of OD and we can have higher pairs rate without sacrificing the bandwidth.

Chapter 2

Six-Wave Mixing

In this chapter, we will describe the proposed SWM scheme. First, we introduce the level scheme of ^{87}Rb, then an overview of the conservation of energy and momentum that characterize the process.

2.1 Proposed Six-Wave Mixing Level Scheme

Similar to FWM, six-wave mixing (SWM) is a parametric process. It is a fifth order non-linear process that involves the interaction of six optical fields in a non-linear medium. We choose to use Rubidium atoms for SWM experiment because the level structure is well studied[23] and the diode lasers to address the optical transitions in Rubidium are easily available in the market.

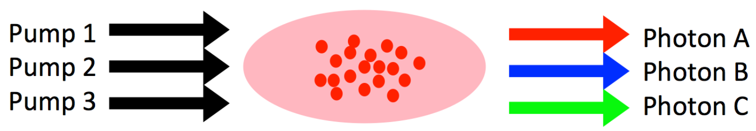

Figure 2.1: Spontaneous six-wave mixing process

The level scheme that we intended to use for six wave mixing is very similar to that one previously used for FWM in our group[9].

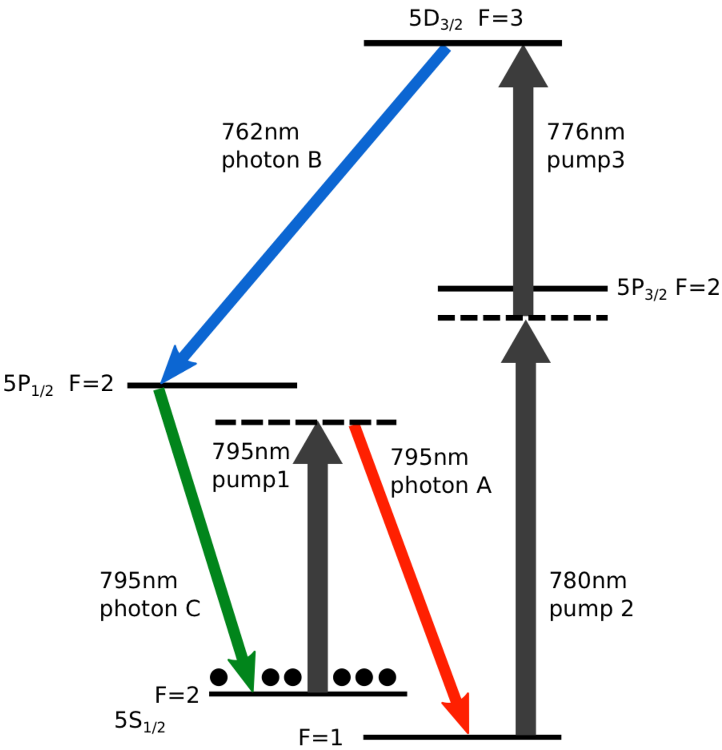

Figure 2.2: Energy level scheme for Six-Wave Mixing process. Initially the atoms are in $5S_{1/2}, F = 2$ ground state, represent by the black dots.

First, the ^{87}Rb atoms in the elongated MOT are prepared in $5S_{1/2}, F = 2$ ground state, the 795nm pump laser excites the atoms to $5P_{1/2}, F = 1$ state follow by a decay to $5S_{1/2}, F = 1$ ground state and emit 795nm photons. The 780nm and 776nm pump laser bring the atoms to $5D_{3/2}, F = 3$ state via two photon excitation. When the atoms decay back to $5S_{1/2}, F = 2$ which is the initial state, 762nm and 795nm photons are emitted. The generated photons that emit in specific directions that are determined by the phase matching condition of this process will exhibit strong time correlation. While in other directions we will only observe uncorrelated fluorescence.

2.2 Phase matching condition

For parametric process such as FWM and SWM, the state of the medium remains the same before and after the interaction. This implies that the energy and momentum must be conserved between the pump and the generated photons. The energy conservation for the SWM mixing process is:

$$\hbar\omega_1 + \hbar\omega_2 + \hbar\omega_3 = \hbar\omega_A + \hbar\omega_B + \hbar\omega_C \tag{2.1}$$

where ω_i is the angular frequency of the field and indices 1, 2, 3 and A, B, C refer to pump and generated photons modes respectively.

The spatially extended ensemble of atoms as non-linear medium for the SWM process posses the translational symmetry which leads to momentum conservation. This conservation is also known as phase matching condition, can be expressed as:

$$\vec{k}_1 + \vec{k}_2 + \vec{k}_3 = \vec{k}_A + \vec{k}_B + \vec{k}_C \tag{2.2}$$

where $\vec{k}_i$ is the wave vector of the field.

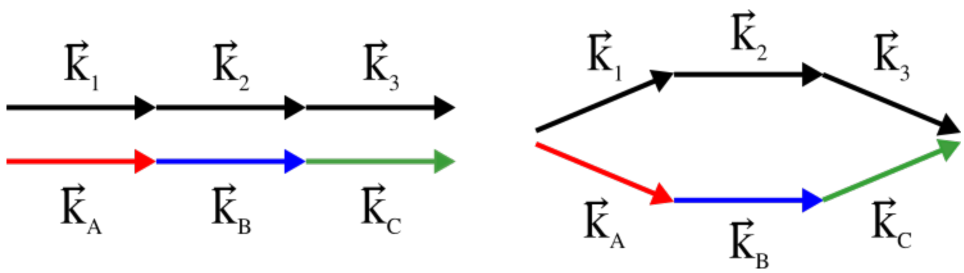

Figure 2.3: Two possible phase matching condition for the pump and generated modes. (Left) Pump and generated modes in collinear geometry (Right) Co-propagating pump and generated modes with angle between them.

There are many solutions to this phase matching condition which give rise to different setups and configurations that we can use to collect the generated photons. This condition is a vector addition where we need to match the sum of the wave vectors between the pumps and the generated photons. Although there are many solutions available, we need to choose a suitable solution with some considerations. We will elaborate more on what solutions we used and the reason we choose them in Chapter 4.

Chapter 3

Laser System and Optical Components

In this section, we will give a brief overview of the necessary optical components in our laser systems and some important atomic transitions in our experiment.

3.1 Optical Components

In our experiments, we need to manipulate the laser light in term of polarization, frequency, direction etc. We will introduce components that help us to modify the light in the way we desire.

3.1.1 Wave Plate

A wave plate is a birefringent material that can modify the polarization of light by creating phase difference for the polarization component along the fast and slow axis. Wave plate is also wavelength dependent as the same wave plate will create different phase difference for light with different wavelength. By varying this phase difference, we can modify the polarization of the light.

- Half Wave Plate (HWP). HWP is a wave plate that creates a phase difference of $\lambda/2$ between the fast and slow axis. HWP can rotate a linear polarization to any other linear polarization.

- Quarter Wave Plate (QWP). QWP is a wave plate that creates a phase difference of $\lambda/4$ between the fast and slow axis. With different orientation of the QWP, we can create elliptically or circularly polarized light from linearly polarized light.

3.1.2 Beam Splitter (BS)

A beam splitter splits incident light at a designated ratio into two separate beams.

3.1.3 Polarizing Beam Splitter (PBS)

Similar to BS, PBS splits the incoming light into two separate beams depending on the polarization. PBS cubes transmit horizontally polarized light and reflect vertically polarized light. A HWP placed between two PBS can be used to control the splitting of the light.

3.1.4 Interference Filter

Interference filter reflects certain spectral bands and transmits others. This filter may be high-pass, low-pass, bandpass or band-rejection. The interference filter that we use in our experiments is MaxLine laser clean-up filter from Semrock which is a bandpass filter. We choose the center wavelength of these filters such that they transmit light that we want to collect. The bandwidth of these filters is 3nm and the transmission around center wavelength is more than 90%. The center wavelength of these filters is angle dependence. When we increase the incidence angle of the light, the center wavelength of the filter will decrease, resulting in partial tunability of the transmitted wavelength.

3.1.5 Electro-Optic Modulator (EOM)

EOM modulates the frequency or phase of incident light with a crystal which has changing refractive index with the presence of electric field. This is achieved by sandwich the crystal with a capacitor and apply a radio frequency (RF) signal to the capacitor, which in turn the oscillating refractive index will modulate the incoming beam.

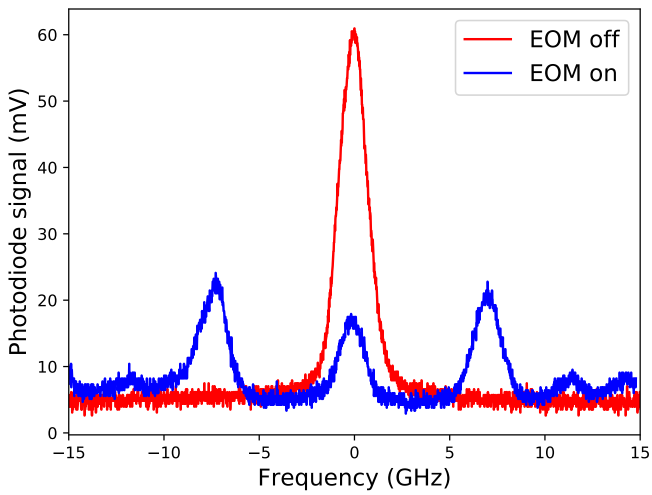

Figure 3.1: The light modulated by EOM is sent through a cavity to observe the sidebands. The modulation frequency is around 7GHz.

The modulated light is sent into a cavity. The transmitted frequency is changed by driving the cavity piezo with different voltage. From Figure 3.1, we can see that the modulation will create two sidebands $\pm\Delta$ away from the laser frequency, where Δ is the frequency of the RF signal we provide.

3.1.6 Acoustic-optic Modulator (AOM)

AOM can modulate both the frequency and direction of a laser. Inside AOM there is a piezoelectric transducer that applies RF acoustic wave to a crystal that changes the crystal refractive index periodically. This effectively creates a diffraction grating which diffracts the incoming beam and changes the frequency of the light depends on the order of diffraction. For the first order diffraction, the outgoing light frequency is $f \pm \Delta$ where f is the incoming light frequency and Δ is the modulation frequency of the AOM.

AOM is a very useful tool in our experiments. Firstly, AOM allows us to modify the light frequency with a range of tens to hundreds MHz by changing the frequency of acoustic wave. Secondly, it can act as a fast light switch by turning on and off the acoustic wave. The switching can be done in less than 1μs.

3.2 External Cavity Diode Laser (ECDL)

We use single-mode semiconductor laser diodes in our experiment. The frequency bandwidth of the laser from these diodes is a few orders of magnitude larger than the natural linewidth of the atom. To address an atomic transition coherently, the linewidth of the lasers should be narrower than the natural linewidth of the transition.

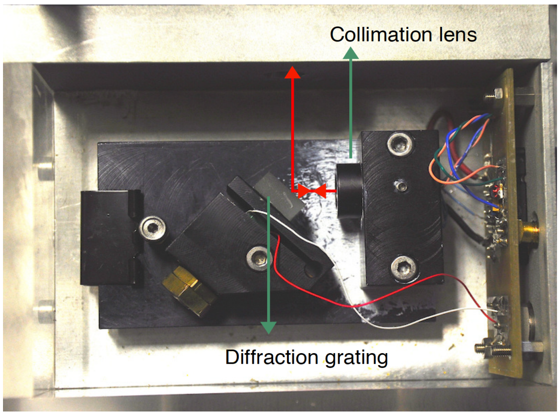

Figure 3.2: The picture of the ECDL in Littrow configuration[5].

We use a grating-stabilised extended cavity in the Littrow configuration as shown in Figure 3.2 to further reduce the bandwidth. This configuration is commonly referred as External Cavity Diode Laser. The external grating us aligned such that the first diffraction order of the laser from the diode is reflected back to the diode as optical feedback while the zero-order beam from grating goes into the experiment. As such, the grating and the diode form an external cavity producing the narrowband laser. The output frequency of the laser changes with the grating angle, temperature and laser current. By changing these parameters, we can roughly tune the frequency to the desired frequency. The linewidth of the laser in this configuration is between 1-2MHz [4, 5].

3.3 Pattern Generator

Pattern generator controls the timing sequence of our experiment. A host computer sends the timing sequence to a home built programmable pattern generator that outputs a serial of electrical signals to control the rest of devices in the setup. In our experiment, this is done by turn on and off the AOM to control the sequence of lasers that we sent in.

3.4 Photodiode

The photodiode we use is PDA36A-EC Si Amplified Detector from Thorlabs. It is an amplified, switchable-gain, silicon detector designed for detection of light signals ranging from 400 to 1100nm. This photodiode is mainly used to detect the sixth generated field from the seeded SWM and operated at 70dB gain since the signal is at the order of nW. The bandwidth of the photodiode operated at 70dB gain is 5kHz.

3.5 Magneto-Optical Trap (MOT)

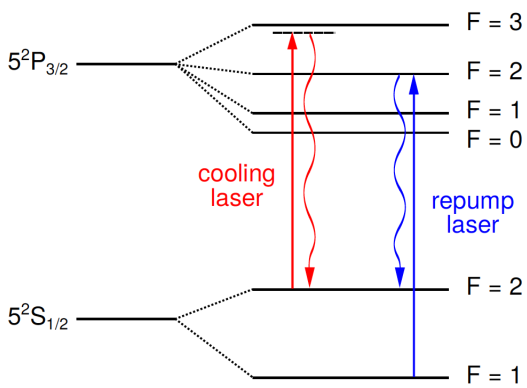

Figure 3.3: The hyperfine energy level of ^{87}Rb D2 line, with the targeted cooling and repump transitions[22].

In order to trap the atoms inside the MOT, we need a cooling laser red detuned from a cyclic transition. This transition is chosen such that the cooling process can undergo many repetitions without fall into any dark states. For our MOT, we choose ^{87}Rb transition from $5S_{1/2}, F = 2$ to $5P_{3/2}, F = 3$ with red detuning of tens MHz. However, there is still a small chance for atoms to go to $5P_{3/2}, F = 2$ state which might decay to the $F = 1$ dark state. As such, we need one repump laser (tuned to $5S_{1/2}, F = 1$ to $5P_{3/2}, F = 2$ transition) to bring the atoms back to the cyclic transition.

Chapter 4

Raman Transition

As discussed in section 2.2, for a given pump geometry, the photon triplets will be generated in well defined spatial modes that satisfy the phase matching condition for this process. For non-collinear geometries, it is difficult to couple the correct spatial modes into single mode fibers without a strong reference signal. We sent in two more seed lasers in addition to the three pump beams to carry out seeded six-wave mixing for alignment purpose.

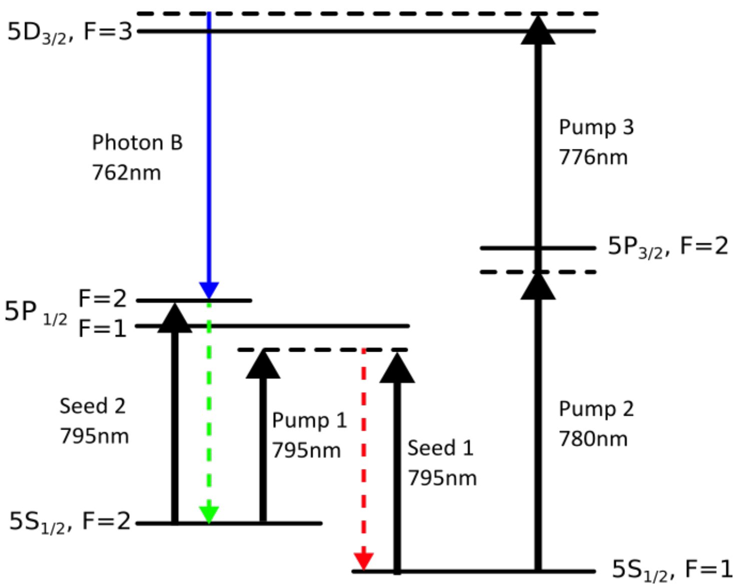

Figure 4.1: Level scheme for seeded Six-Wave Mixing process. The dotted lines represent stimulated emission process.

The seeded SWM acts as a parametric amplifier where the seed lasers induce stimulated emission in two of the decay channels. With 5 beams on at the same time, the sixth field which has a wavelength of 762nm can be observed macroscopically with a photodiode or CCD camera. The presence of the 762nm signal also served as a shred of evidence that this whole SWM process works since no one has done SWM with this level scheme before.

4.1 Stimulated Raman Transition

Lets us have a closer look at the SWM level scheme, the atoms are initially prepared at $5S_{1/2}, F = 2$ ground state and then transferred to $5S_{1/2}, F = 1$ via two 795nm lasers. This transition between the two ground states through $5P_{1/2}, F = 1$ excited state is called stimulated Raman transition[26]. To have an efficient transfer of atoms from the initial state to the other ground state, it is important for us to study the relevant parameters for our experiments.

4.1.1 Theory

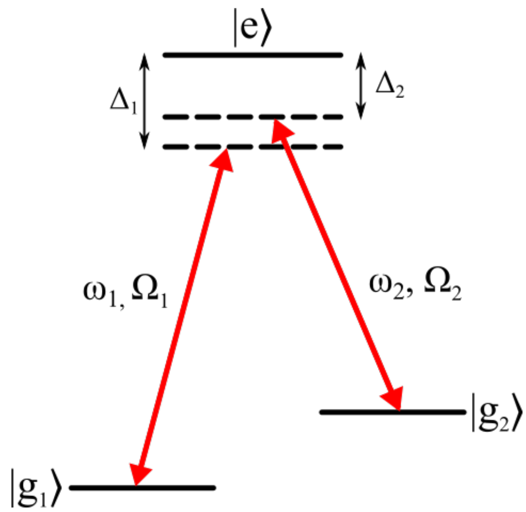

Figure 4.2: Basic scheme of a stimulated Raman system. The two ground states $|g_1\rangle$ and $|g_2\rangle$ are coupled to each other through the excited state $|e\rangle$. This is done by two separate lasers, each coupling a different ground state to the excited level.

Stimulated Raman transitions provide a method to drive coherent transitions between the two ground states while reducing spontaneous emission from the excited state by using two coupled lasers. Consider the three level system shown in Figure 4.2. One laser couples the state $|g_1\rangle$ to the excited state $|e\rangle$ with laser frequency ω_1 while the other laser couples the state $|g_2\rangle$ to the same excited state with laser frequency ω_2. The detuning of these two lasers from resonance is Δ_1 and Δ_2 respectively.

The Hamiltonian of this system in the interaction picture is given by[26]

$$H = -\sum \left(\omega_k |g_k\rangle \langle g_k| + \frac{\Omega_k}{2} e^{i\omega_k t} |g_k\rangle \langle e| + \frac{\Omega_k^*}{2} e^{-i\omega_k t} |e\rangle \langle g_k| \right) \tag{4.1}$$

where we have assumed the zero point energy to be the excited state energy. Note also we have taken the rotating wave approximation and ignored additional laser couplings.

This Hamiltonian can be transformed into an effective Hamiltonian[26] as

$$H_{\text{eff}} = \begin{pmatrix} \frac{|\Omega_1|^2}{4\Delta} - \frac{\delta}{2} & \frac{\Omega_1 \Omega_2^*}{4\Delta} \\ \frac{\Omega_1^* \Omega_2}{4\Delta} & \frac{|\Omega_2|^2}{4\Delta} + \frac{\delta}{2} \end{pmatrix} \tag{4.2}$$

where Δ is defined such that $\Delta = \frac{\Delta_1 + \Delta_2}{2}$ and for δ which is the two photon detuning, $\Delta_1 = \Delta - \frac{\delta}{2}$ and $\Delta_2 = \Delta + \frac{\delta}{2}$.

We can incorporate the $\frac{\Omega_k^2}{4\Delta}$ terms into the defination of energy and define the Raman frequency as

$$\Omega_R = -\frac{\Omega_1^* \Omega_2}{2\Delta} \tag{4.3}$$

such that the effective Hamiltonian will become

$$H_{\text{eff}}^{'} = -\frac{1}{2} \begin{pmatrix} \delta & \Omega_R^* \\ \Omega_R & -\delta \end{pmatrix} \tag{4.4}$$

and this is just the usual Hamiltonian that describes a two levels system coupled to a laser field. As such, Raman transition of a three levels system can be described as an effective two levels system.

The terms $\frac{\Omega_k^2}{4\Delta}$ that we incorporated earlier are simply the AC stark shifts caused by the laser fields themselves. Furthermore, we did not take into account the additional shifts such as coupling between states $|g_1\rangle$ and $|e\rangle$ induced by laser 2. Such coupling will give rise to additional AC stark shifts. In general, we have to account for all these shifts when finding resonance frequency for the two photon transition to have as much population being transferred as possible.

4.1.2 Steady State Population

Follow the usual treatment for two levels system coupled with a laser field[26] using the effective Hamiltonian above, we are interested in the steady state population to have an efficient Raman transfer to the other ground state. The steady state population for two levels system is given by[26]:

$$\rho_{ee} = \frac{1}{2}\frac{s_0}{1 + s_0 + 4\Delta^2/\Gamma^2}, s_0 = \frac{2|\Omega|^2}{\Gamma^2} \tag{4.5}$$

where Δ is the detuning and Γ is the linewidth of the transition. Replace Δ with δ and Ω with Ω_R such that this become steady state population for the "excited" state for the Raman transition.

From the above relation we can see that, in order to have higher excited state population, δ has to be as small as possible while Ω_R which is proportional to laser intensity has to be as large as possible.

4.1.3 Splitter setup

The two lasers we use to drive the Raman transition in our experiment are originated from the same laser which has a wavelength of 795nm. The advantage of doing so is that these lasers are automatically in phase. The setup is shown in Figure 4.3:

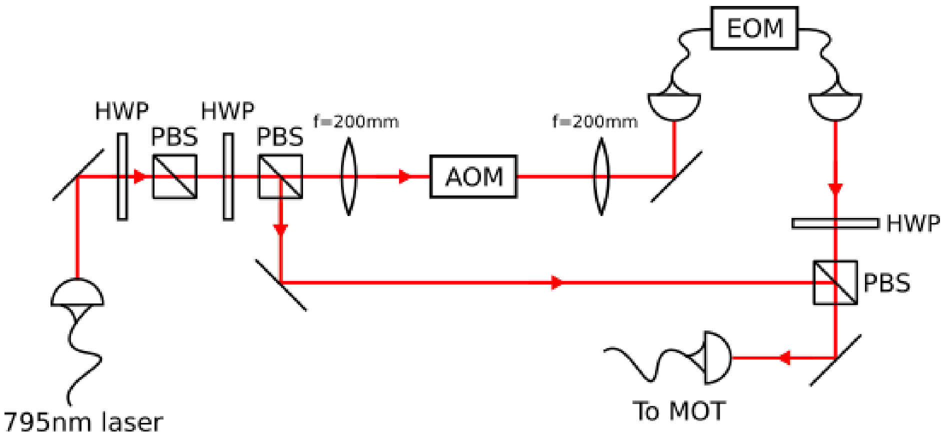

Figure 4.3: Schematic of the splitter setup. The lasers are then combined using PBS and coupled into a single mode fibre.

The laser power in each arm after the PBS can be controlled by adjusting the HWP. If we sent the laser light directly into the EOM, the frequency we get is f and $f \pm \Delta$ where f is the laser frequency and Δ is the modulation frequency. With these three laser frequencies, the two possible Raman transitions that will occur are shown in Figure 4.4 below.

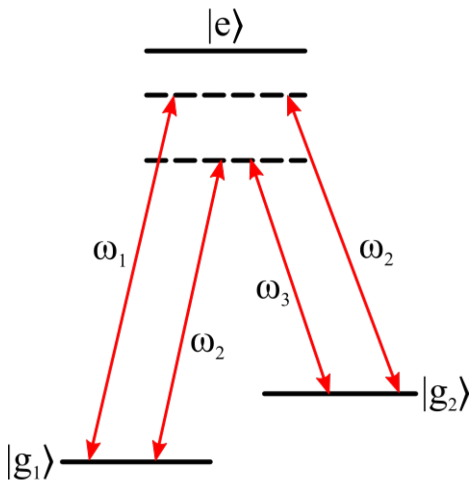

Figure 4.4: Schematic of the two possible Raman transitions with three laser frequencies that are equally spaced, where $\omega_1 - \omega_2 = \omega_2 - \omega_3 = \Delta$.

In order to eliminate other Raman transitions that may occur, we want to have only two laser frequencies with frequency separation of 6.8GHz that match the separation between the $F = 1$ and $F = 2$ ground state[23]. While all other frequency separation other than 6.8GHz will result in a non-zero δ, where δ is the two photon detuning. We first sent the laser into AOM to get an offset of 200MHz. After that, the minus first order of the diffracted laser is coupled into the EOM. At this point, the frequencies we have are $f-200$MHz $f\pm\Delta-200$MHz. We set the modulation frequency to 7GHz. The resulting frequencies will be $f-200$MHz, $f-7.2$GHz and $f+6.8$GHz. As such, we are able to get the 6.8GHz frequency separation between the two lasers.

4.1.4 Blue fluorescence

As mentioned in section 4.1.1, we need to account for AC stark shift. We optimise the Raman transition by looking at how well the atom is being transferred to the other state as this procedure automatically takes into account all shifts. We use the blue fluorescence emitted by the atomic cloud as an indication of the efficiency of the Raman transition. We sent in 4 lasers which are 795nm, 780nm, 776nm pump lasers and 795nm seed laser 1 collinearly into the atomic cloud. If the atom is being transferred to $5S_{1/2}, F = 1$ state, it will be excited to $5D_{3/2}$ state via two photon excitation induced by the two pump lasers. At this state, the atom can decay to $6P_{3/2}$ state and then decay again back to $5S_{1/2}$ ground state by emitting a photon which has a wavelength of 420nm.

Although the blue fluorescence is an indirect indication that the atom has been transferred to the $F = 1$ ground state, the advantages of doing so is that it is easier to detect blue fluorescence because the wavelength is very different from all the lasers and scattering light which are around 780nm in wavelength.

(a) Atomic cloud without sent in any pump and seed laser.

(b) Atomic cloud when sent in 780nm and 776nm pump lasers.

Figure 4.5: Comparison of the atomic cloud.

When we send in the lasers in CW mode, we observe blue fluorescence even when we block the Raman lasers. As mentioned in section 3.5, the atom has a certain probability to fall into $5S_{1/2}, F = 1$ state during the cooling cycle which then will be excited by the 780nm and 776nm pump lasers to $5D_{3/2}$ state. To address this problem, we need to have a duty cycle for the whole process. The cycle is shown below:

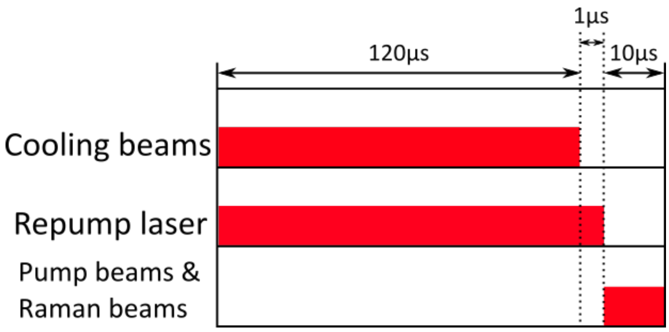

Figure 4.6: Experiment timing sequence controlled by pattern generator.The pattern generator will sent signal to switch the corresponding AOM on and off.

Using this duty cycle with repump laser turn off later than cooling laser, we can make sure that most of the atoms are in $5S_{1/2}, F = 2$ state. When we block any of the Raman lasers, the blue fluorescence will disappear as an indication that the atoms are in $F = 2$ state. We detect this fluorescence using a blue filter and a CCD camera, the setup is as shown below:

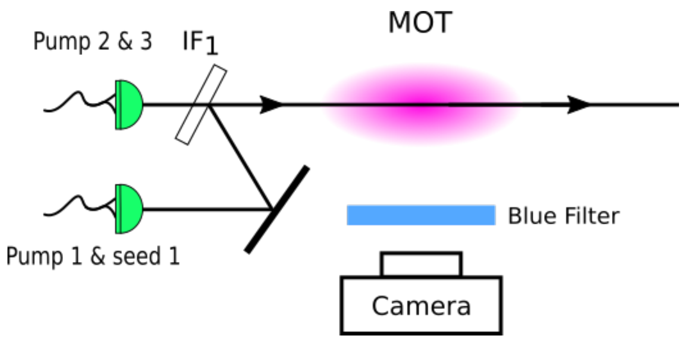

Figure 4.7: Schematic of the experimental setup to observe the blue fluorescence. The filter is BG39 colored glass bandpass filter where the bandpass region is 360 to 580 nm.

We set the Raman lasers to be 400MHz red-detuned from $5P_{1/2}, F = 1$ state and this is done by a double pass 200MHz AOM. Since the detuning is very large, the blue fluorescence is expected to be very weak and we need to set the shutter time of camera to 1s to pick up the signal. The CCD camera we use is Chameleon3 CCD camera (Sony ICX445) from Pointgrey. It has a resolution of 1288 $\times$ 964 pixels with a pixel size of 3.75μm. We also adjust the power ratio of Raman lasers by rotating the HWP to get the brightest signal. The optimum power for 795nm pump and seed laser 1 is 2.2mW and 590μW respectively.

With this signal, we start to measure the effect of Raman laser power on the blue fluorescence. First, we change the seed 1 laser power by changing the power of AOM and take pictures using the camera. The brightness is obtained by adding up the number of each pixel which is proportional to intensity. Next, we use a variable neutral density (ND) filter to vary the power of the pump laser and repeat the same measurement. The result is shown below:

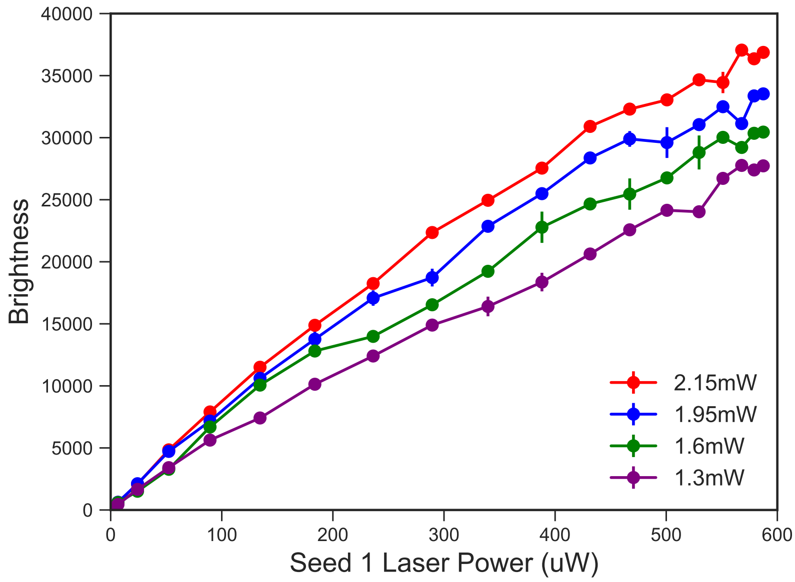

Figure 4.8: Brightness of blue fluorescence at different pump and seed laser power. The different pump power is represented by different colour. The 780nm pump power is 950μW and 776nm pump power is 24mW.

From the graph above, we observe that the brightness of the blue fluorescence increase when we increase the power of pump or stoke laser. This observation agrees with the steady state population equation 3.5. As Ω_R^2 is proportional to the power of both lasers, when the power is below the saturation power, the population increase linearly with the power of lasers. This result also shows that we are not limited by the power of 780nm and 776nm pump lasers. This is because the increase in population will not increase the brightness if it is limited by the 780nm and 776nm pump power.

Chapter 5

Seeded Six-Wave Mixing

In this chapter, we present the seeded six-wave mixing. We pump the atomic cloud with 5 laser beams sent into the atomic cloud and observe the generation of a sixth field. We also carry out the seeded SWM with different configurations and compare the signal obtained.

5.1 Seeded Six-Wave Mixing with Collinear Configuration

In this section, we will focus on the seeded SWM with collinear configuration.

5.1.1 Experimental Setup and Alignment Procedure

For the SWM process, collinear configuration gives us the most simple solution to the phase matching condition since all the generated photons have to be emitted in the same direction as the pump photons. Consider that the atomic cloud we have is elongated, by sending all the pump beams in along the elongated axis of the atomic cloud will result in more atoms interact with the pump beams. The collinear configuration for seeded SWM is shown as below:

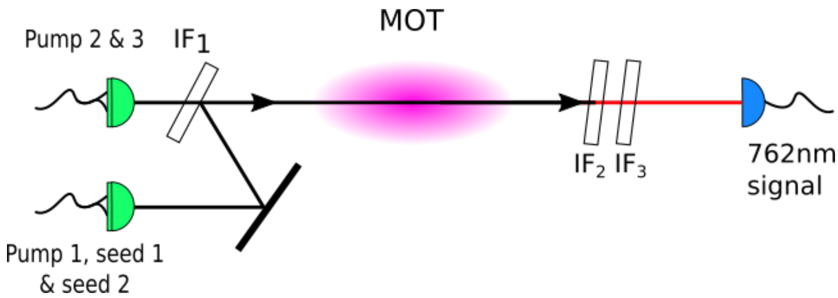

Figure 5.1: Schematic of the collinear setup for seeded six-wave mixing process.

To get the optimum overlap and spatial mode of the lasers, we first optimize the alignments by doing seeded FWM. We tuned the 780nm pump laser to be on resonance with $F = 2 \rightarrow F' = 3$ transition and only sent in 780nm pump, 776nm pump and 795nm seed 2 laser. Since the signal is 762nm in wavelength, it can be easily separated out from the pump lasers using interference filters. We used two interference filters (IF_2, IF_3) to have enough extinction to get rid of the pump lasers. We then adjust the direction and focus of the laser beams to maximize this signal on the photodiode.

Next, we tuned the 780nm pump laser back so that it is on resonance with $F = 1 \rightarrow F' = 2$ transition and sent in all the pump and seed lasers. The raman detuning is set to zero for this seeded process. A similar duty cycle is used for this process with 1500μs of cooling and repump laser on follow by 85μs of pump and seed lasers on. The timing sequence of the cycle is controlled by pattern generator which sent electrical signals to switch the AOM on and off. We observe the generated 762nm using a photodiode. To make sure that this signal is generated by the seeded SWM process, we block every laser one by one and check on the signal. As such, we can confirm that this signal is indeed produced by the seeded SWM process. We continue to optimize the signal by changing the polarization and power of each laser.

5.1.2 Results

The following figure is the signal recorded by oscilloscope triggered by the pattern generator.

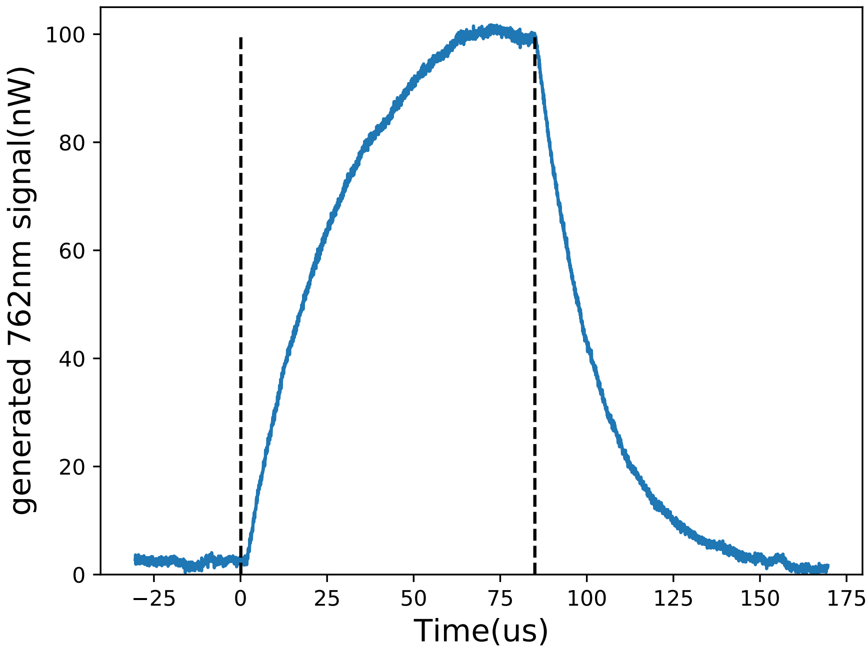

Figure 5.2: Generated 762nm signal collected using a photodiode connected to oscilloscope. The oscilloscope is triggered on the time window where the pump and seed lasers are on. The dotted line indicate the time where we switch on and off the pump and seed lasers.

During the optimization process, we found out that the optimum power for certain lasers is not necessarily the maximum power. We measured how the power of the lasers affect the 762nm signal strength. We choose 780nm pump and 795nm seed 2 laser for this measurement.

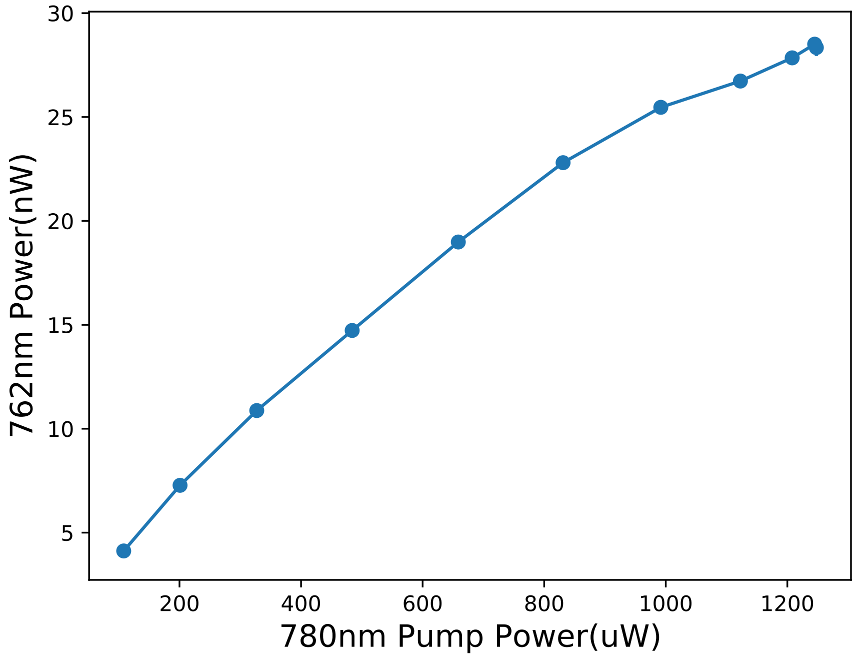

Figure 5.3: Graph of 762nm signal strength at different 780nm pump power while the power of the remaining lasers are kept constant. The errorbar of the data points is too small to be seen in this graph. 776nm pump: 24mW, 795nm pump: 2.66mW, 795nm seed 1: 870μW, 795nm seed 2: 105μW.

The power of the pump laser is controlled by changing the RF power that supplies to the AOM. From the graph above, we can see that the 762nm signal increase when the 780nm pump power increase but no saturation effect has been observed. This means that the signal strength can be further increased by higher pump power.

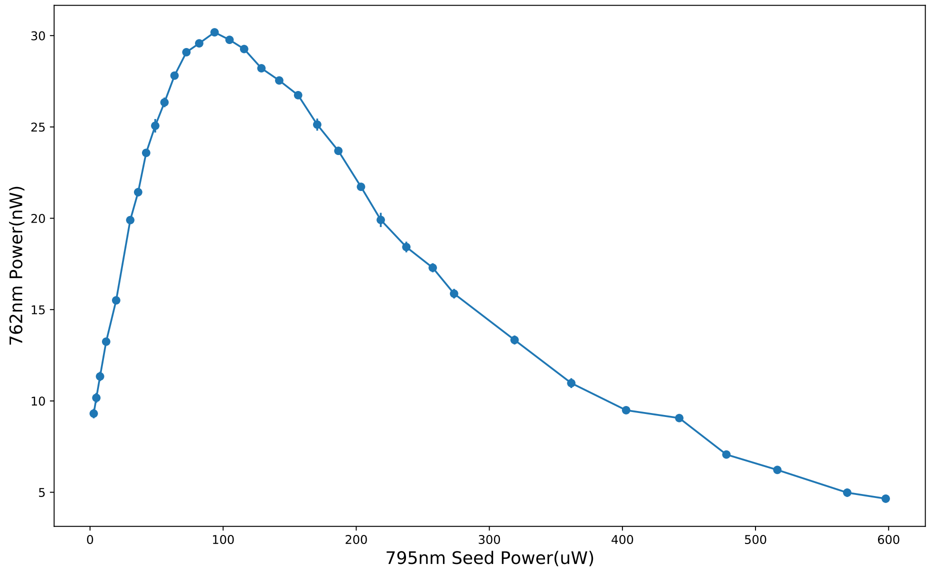

Figure 5.4: Graph of 762nm signal strength at different 795nm seed 2 power while the power of the remaining lasers are kept constant. The errorbar of the data points is too small to be seen in this graph. 780nm pump: 1.25mW, 776nm pump: 25mW, 795nm pump: 2.78mW, 795nm seed 1: 940μW.

From the graph above, we observe the same behaviour as in Figure 5.3 when the power of 795nm seed 2 is lower than 100μW. When the power increase beyond 100μW, the 762nm signal started to drop and become lower than the beginning.

The 795nm seed 2 laser is on resonance with $F = 2 \rightarrow F^{'} = 2$ transition, the light will scatter away the atoms easily and the beam will penetrate the atomic cloud at high power. As such, lesser atoms participate in the seeded SWM process which results in the drop of the 762nm signal.

5.2 Seeded Six-Wave Mixing with Counter-Propagating Configuration

Although the collinear configuration is the most simple setup and we are able to observe the 762nm signal generated by the seeded SWM process, there is a problem that we will face with this configuration. Notice that in the SWM process, there are two generated photons and one pump beam have wavelength of 795nm. In term of frequency difference, the two generated photons are just 800MHz and 6.8GHz respectively away from the 795nm pump laser. As such, we cannot separate them using interference filter as before. Better filtering optics such as cavity has to be used in order to separate these photons from the pump. However, we need at least two cavities or more if the cavity does not have enough extinction to get rid of the pump lasers. As such, we decided to find a different phase matching condition that can help us to separate the photons spatially.

5.2.1 Phase Matching Condition for Counter-Propagating Configuration

As the atomic cloud in our MOT is elongated, we hope to have a configuration that all the pump beams pass through the cloud along the elongated axis in order to have maximum interaction volume. We sent the 795nm pump laser in from opposite direction as the other two pump lasers. Next, we set the emission direction of the 762nm photon to be same as the 780nm and 776nm pump beams and calculate the emission direction of the remaining photons. In the coordinate which direction of the 780nm pump is zero, the emission direction for photon A and photon C is -38.14° and 141.86°. These two photons will be emitted in almost opposite direction and the difference is less than 0.001°. Figure 5.5

illustrates how this configuration looks like.

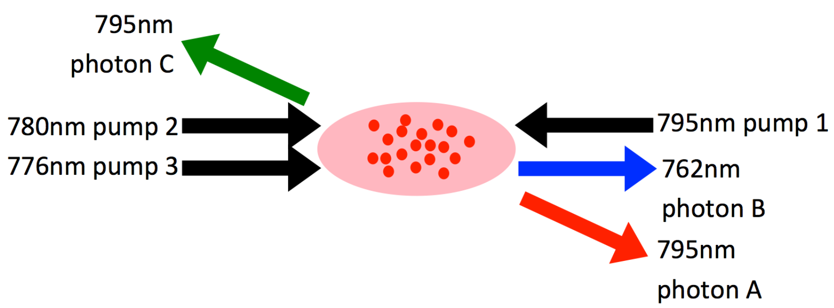

Figure 5.5: Counter-propagating phase matching condition which allow us to spatially separate the generated photons which have similar wavelength.

Next, we try to vary the emission angle of photon A and calculate how the emission angle of the remaining photons change with it.

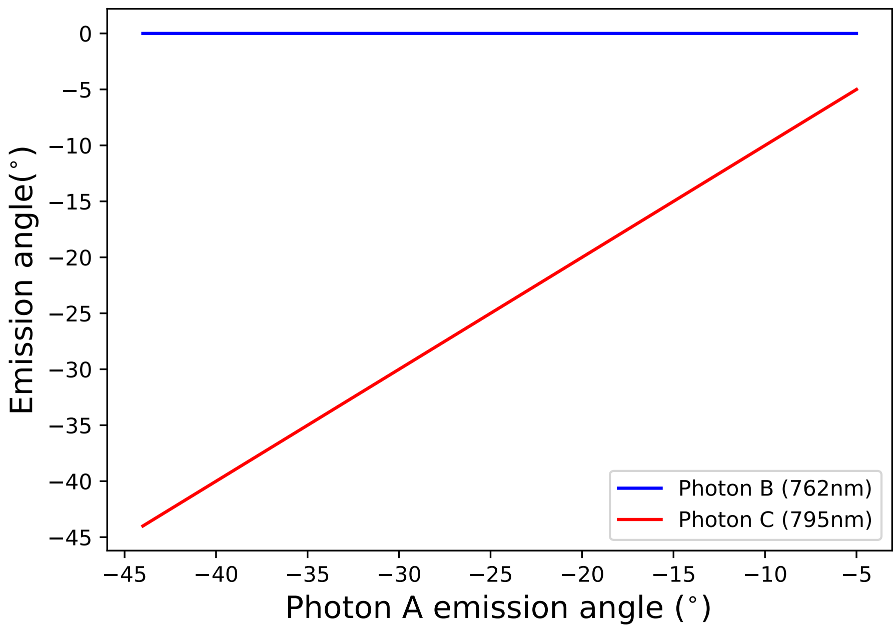

Figure 5.6: Change of emission angle of photon B and C as a function of emission angle of photon A. Photon B remains in almost same angle with different emission angle of photon A and C. The emission angle of photon C is plotted with a constant angle difference of 180°.

In the graph above, the emission angle of photon C is plotted with a constant angle difference of 180° for a clearer comparison with photon A. There are a few observations that can be made from this result. Firstly, photon A and photon C will emit in exactly opposite direction for a wide range of angle. Secondly, the emission direction of photon B almost remains unchanged throughout angle change of 40°. In fact, the emission angle of photon B only changes by 0.003° which is extremely small.

This result shows that this configuration is very flexible where we only need to send in the two 795nm seed lasers from opposite direction and the 762nm photon will be emitted in the same direction as 780nm pump beam. Another advantage of this configuration is that as the two seed lasers are exactly opposite of each other, the fibers for these two lasers can be used for both delivery and collection of light.

5.2.2 Experimental Setup and Alignment Procedure

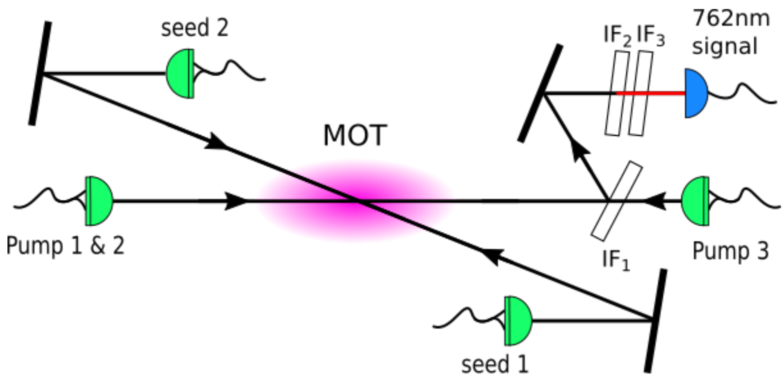

Figure 5.7: Schematic of the counter-propagating setup for seeded six-wave mixing process. IF: interference filter

Figure 5.7 shows the setup for the counter-propagating configuration. First, the 795nm pump laser is coupled back into the fibre that sent the 780nm and 776nm pump lasers in. Next, the 795nm seed 1 laser is aligned to pass through the atomic cloud by maximizing the blue fluorescence signal. While the last 795nm seed 2 laser is aligned by coupled back to the seed 1 laser to get better overlapping between these two beams. The angle between the two seed lasers and the pump lasers is approximately 15°. The interference filter IF_1 is aligned such that it transmits light of 795nm in wavelength. As such, the 780nm, 776nm pump and generated 762nm will be reflected and the 762nm light is collected after the filter IF_2 and IF_3.

5.2.3 Results and Comparison

The 762nm signal detected in both configuration is shown and compared in Figure 5.8:

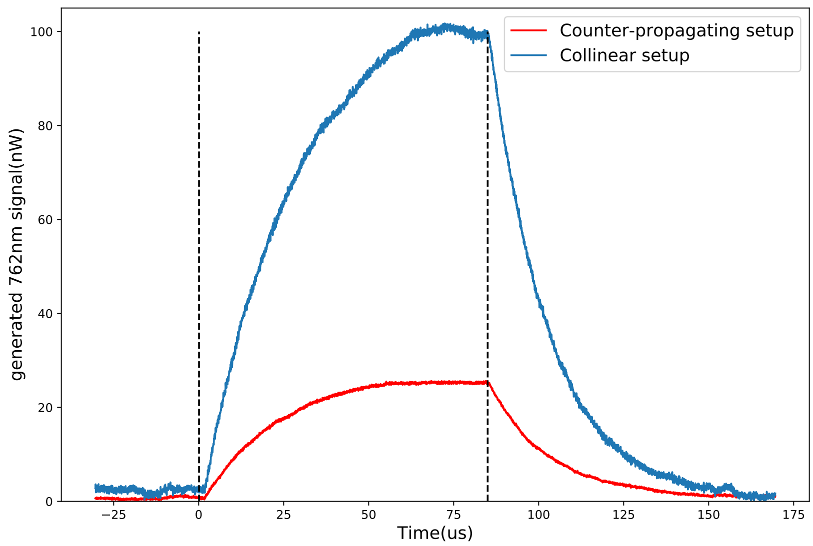

Figure 5.8: Comparison of 762nm signal generated from two different configurations. The two signals have similar shape with different amplitude.

From the comparison above, we can see that the signal generated using counter-propagating setup is about four times lower than the signal for collinear setup. This is due to the decreasing in interacting volume between the atomic cloud and the lasers when the seed lasers are sent into the cloud at an angle. Next, the imperfection in overlapping all the lasers also contribute to the decrease in signal strength.

We also check the spatial mode of the generated signal using a CCD camera.

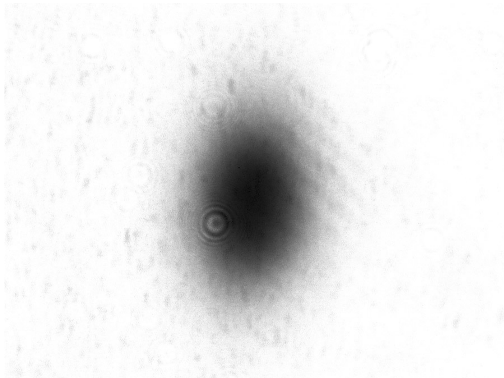

Figure 5.9: Mode of generated 762nm beam collected using a camera.

From Figure 5.9 we can see that the generated mode is nearly Gaussian with an elongated vertical axis and it is coupled into a single mode fibre with a coupling efficiency of 85%.

5.2.4 Seeded SWM with different seed laser

We proceed to collect the generated photon and see if there is any correlation between them. The collection sites for the generated 795nm photon have already been in place since these photons will emit in the opposite direction. However, we did not observe any correlation between the photon collected using avalanche photodiode (APD).

Next, we try to carry out the seeded SWM with different combination of seed lasers. The reason for doing this is that we want to observe correlated photon pairs with only one seed laser on since we did not observe correlated photon triplets. If we want to do it with one of the 795nm seed lasers, the generated 795nm photon will emit in the opposite direction as the 795nm seed laser. We can use BS to reflect the generated photon and couple it into fiber by the seeded process. If we decide to do it with the 762nm seed laser, this seeded process will help us to optimise the power and frequency of the 762nm seed laser.

The 762nm seed laser is locked at the transition from $5P_{1/2}, F = 2$ to $5D_{3/2}, F = 3$ and is sent in from the same direction as 780nm pump laser. While the emission direction of the photon C is opposite of the seed 1 laser, we place a 50:50 BS to reflect the generated photon C so that we can detect it with a photodiode.

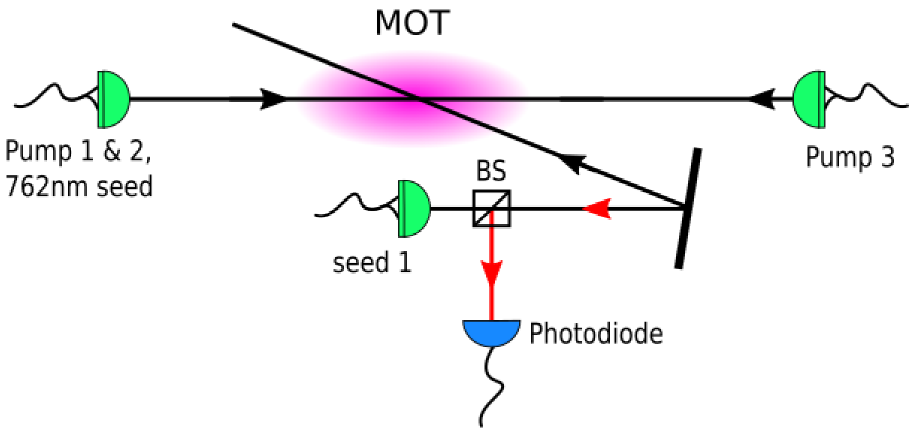

Figure 5.10: Schematic of the counter-propagating setup for seeded SWM with different seed lasers. The generated signal is separated from the seed laser with a beam splitter and detected with photodiode.

By adjusting the alignment and frequency of 762nm laser, we observe a similar signal as the generated 762nm signal as before. This generated 795nm disappear when we block any of the pump and seed lasers.

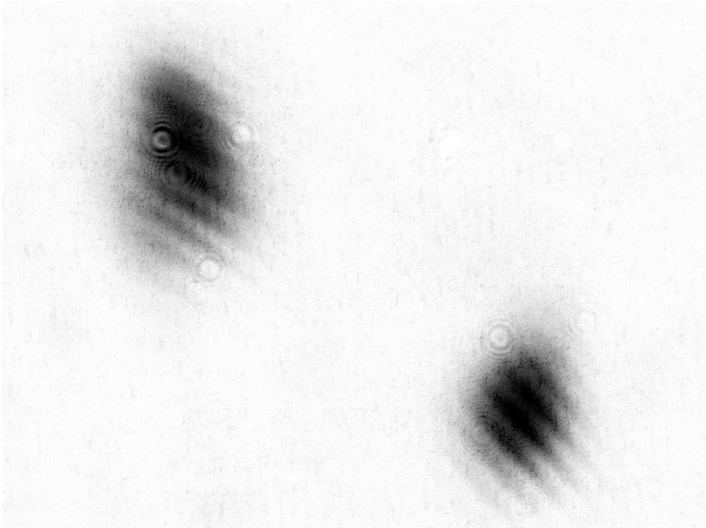

Figure 5.11: Two different modes generated from FWM and SWM. The upper left mode has wavelength of 795nm while the lower right mode has wavelength of 780nm.

When we look at the spatial mode of this signal on the camera, we observe two modes appear on the camera as shown Figure 5.11. The mode located at the upper left vanish when we block any of the pump and seed lasers while the other one vanishes only when we block the 780nm pump, 795nm pump and seed 1 lasers. The wavelength of these modes can be easily identified using interference filter. The upper left mode has a wavelength of 795nm while the other has a wavelength of 780nm.

5.3 Competing FWM

Looking back at the level scheme of SWM, this extra mode probably is generated from a competing FWM process as shown in figure below:

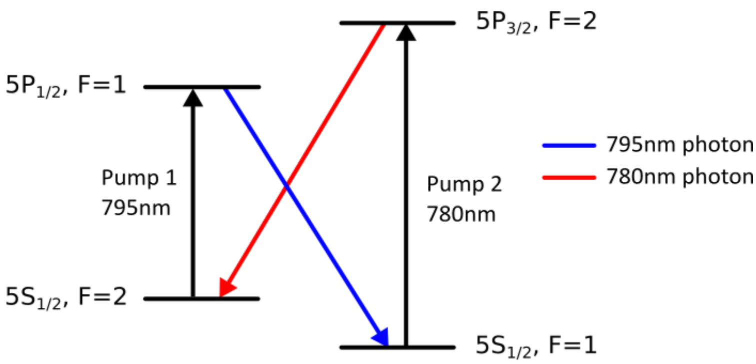

Figure 5.12: Level scheme of four-wave mixing process within the six-wave mixing process.

The 780nm photon generated by this process can be filtered away using interference filter. However, The 795nm photon generated by the FWM has exactly the same frequency and spatial mode as the one generated by the SWM process. This means that we cannot separate them using any filtering optics.

Since we cannot distinguish the photon generated by both processes, we try another approach to address this problem which is to eliminate this FWM process, or at least decrease the rate of this FWM such that it is far more lower than the rate of SWM process.

In order to achieve this, we need to find a suitable power and detuning for 780nm pump laser such that more atom is being pumped to $5D_{3/2}$ state instead of decay to $5S_{1/2}, F = 2$ state which will subsequently contribute to the FWM process. We investigate this by looking at the 780nm scattering light and blue fluorescence emitted from the atomic cloud. Ideally, when the detuning increase, we hope to observe that the blue fluorescence decrease at a rate slower than the decreasing in 780nm scattering.

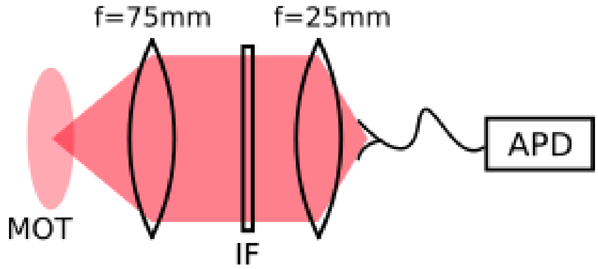

Figure 5.13: Schematic of the scattering light collection setup.

The collection setup is shown in Figure 5.13. The scattering light from the atomic cloud can be treated as it was emitted from a point source. We use a lens to collimate the light and a second lens to focus it into a multi-mode fibre. This fibre is then connected to a APD. Similar to the experiment in the previous section, a duty cycle is used for this measurement. The APD is connected to a coincidence board which act as AND gate so that only counts within the window where pump lasers are switched on will be registered. As such, the 780nm scattering light during the cooling window which caused by the cooling laser will not be registered. The result is shown in the graph below:

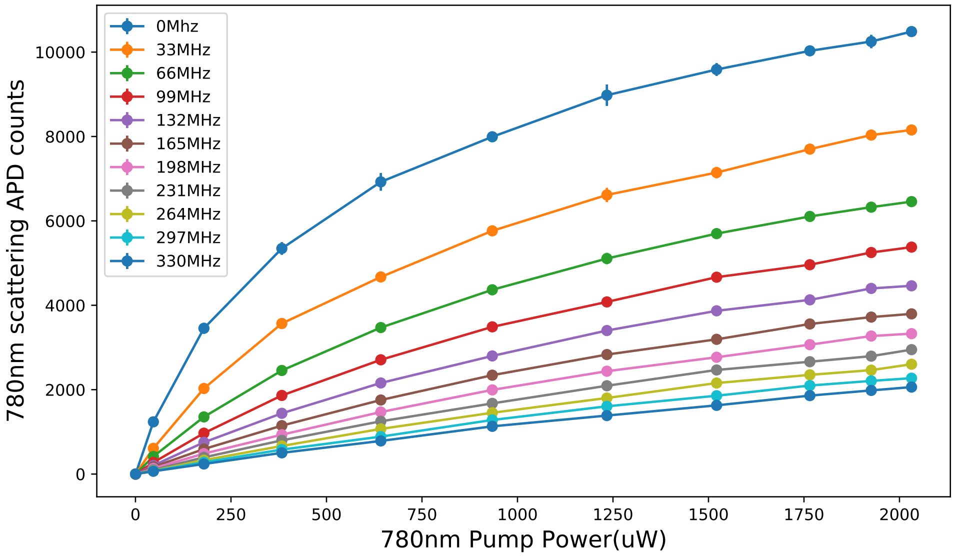

Figure 5.14: Graph of 780nm scattering light against 780nm pump power at different detuning. The detuning show in the graph is red-detuning from the $5P_{3/2}, F = 1$ state.

In this measurement, we used Eagleyard distributed feedback (DFB) laser as the frequency of this laser change linearly with the current supply to it. As a result, we can achieve a large and continuous detuning range of a few hundred MHz which is hard to achieve with AOM. The result in Figure 5.14 agrees with our expectation where the scattering light will increase with pump power and decrease with detuning. Next, we repeat the measurement with blue fluorescence. This is done by changing the interference filter to a blue filter where we used to in the previous experiment.

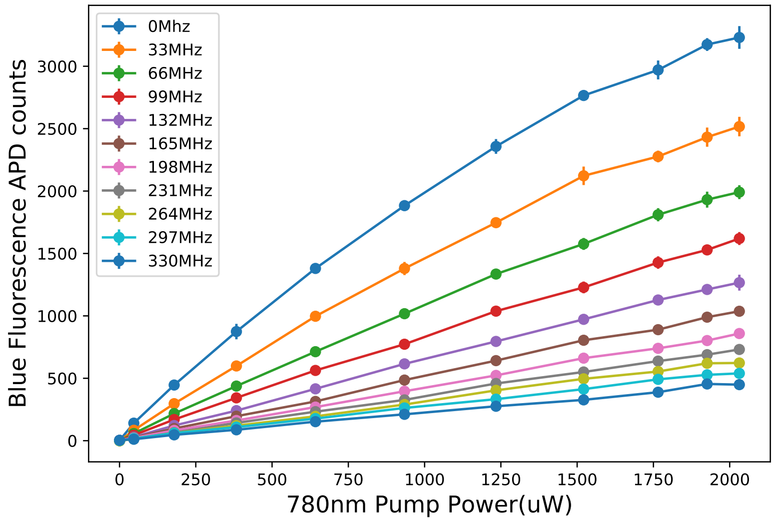

Figure 5.15: Graph of 780nm scattering light against 780nm pump power at different detuning. The detuning show in the graph is red-detuning from the $5P_{3/2}, F = 1$ state.

The above result is similar to the previous measurement. Now we compare these two results at same 780nm pump power. We fit the result to calculate the dependence of the scattering light on detuning.

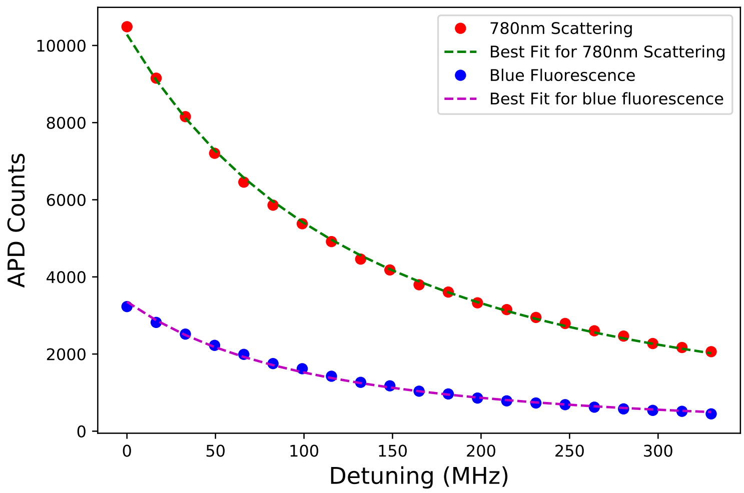

Figure 5.16: 780nm scattering and blue fluorescence at 780nm pump power of 2.03mW. We fit the data using $1/x^2$ where x is the detuning. The reduced chi-square for 780nm scattering and blue fluorescence is 1.026 and 1.464 respectively.

Initially, we hope the 780nm scattering light and blue fluorescence scale differently with respect to detuning such that the 780nm scattering light will decrease at a faster rate compared to blue fluorescence. However, the results show that both signals is inversely proportional to detuning square.

Chapter 6

Conclusion and Outlook

We started this thesis by proposing a six-wave mixing scheme to generate correlated photon triplets. We have described the theory and setup of Raman transition which is the key step towards the seeded six-wave mixing. We have observed the blue fluorescence as an indication that the Raman transfer indeed occur and the transfer rate is proportional to the power of the Raman lasers.

Next, we carry out the seeded SWM with 5 lasers on in a collinear configuration. The sixth field which has 762nm in wavelength has been observed using photodiode with the signal strength of around 100nW. However, it is technically challenging for us to separate the generated photons from the pump beams during actual SWM because some of the pump and generated photon have very similar frequencies that are only a few GHz apart.

We find a different solution to the phase matching condition that can help us to separate the generated photon from the pumps spatially. In this counter-propagating configuration, we sent in 795nm pump laser from the opposite direction from the other two pump lasers. The two 795nm seed lasers are sent into the atomic cloud at an angle of 15° with respect to the pump lasers. The generated sixth field is observed in the same direction as the 780nm pump laser with both photodiode and CCD camera. The 762nm beam generated in this configuration has a power of 25nW which is four times lower than the signal generated in collinear configuration. This is due to the decreasing in interacting volume between the lasers and the atomic cloud. While this generated 762nm mode is nearly Gaussian.

However, when we carry out seeded SWM with 762nm seed laser, using a CCD camera we observed an extra mode generated by a competing FWM process. We start to study how the system reacts to different power and detuning of 780nm pump laser hoping to reduce this FWM process. We collected the 780nm scattering light and blue fluorescence from the cloud for different power and detuning of the 780nm pump. Unfortunately, these scattering light scale in the same way with respect to the detuning at constant pump power.

The next step of this experiment is to carry out seeded SWM with one seed laser remove. We hope to observe photon pairs with time-correlation. In order to achieve this, we need to study the system more in order to get rid of all the uncorrelated scattering.

Bibliography

[1] M. A. Nielsen and I. L. Chuang, *Quantum computation and quantum information.* Cambridge university press, 2010.

[2] A. K. Ekert, "Quantum cryptography based on bell's theorem," *Physical review letters*, vol. 67, no. 6, p. 661, 1991.

[3] V. Leong, M. A. Seidler, M. Steiner, A. Cerè, and C. Kurtsiefer, "Time-resolved scattering of a single photon by a single atom," *Nature communications*, vol. 7, p. 13716, 2016.

[4] B. Srivathsan, *Heralded Single Photons for Ecient Interaction With Single Atoms.* PhD thesis, National University of Singapore, 2014.

[5] G. K. Gulati, *Narrowband Photon Pairs From a Cold Atomic Vapour for Interfacing With a Single Atom.* PhD thesis, National University of Singapore, 2015.

[6] M. Steiner, V. Leong, M. A. Seidler, A. Cerè, and C. Kurtsiefer, "Photon bandwidth dependence of light-matter interaction," *Opt. Express*, vol. 25, pp. 6294–6301, Mar 2017.

[7] T. Chaneliere, D. Matsukevich, S. Jenkins, S.-Y. Lan, T. Kennedy, and A. Kuzmich, "Storage and retrieval of single photons transmitted between remote quantum memories," *Nature*, vol. 438, no. 7069, p. 833, 2005.

[8] C. Kurtsiefer, M. Oberparleiter, and H. Weinfurter, "High-efficiency entangled photon pair collection in type-ii parametric fluorescence," *Phys. Rev. A*, vol. 64, p. 023802, Jul 2001.

[9] B. Srivathsan, G. K. Gulati, B. Chng, G. Maslennikov, D. Matsukevich, and C. Kurtsiefer, "Narrow band source of transform-limited photon pairs via four-wave mixing in a cold atomic ensemble," *Physical review letters*, vol. 111, no. 12, p. 123602, 2013.

[10] T. Cheng, L. Zhang, X. Xue, D. Deng, T. Suzuki, and Y. Ohishi, "Broadband cascaded four-wave mixing and supercontinuum generation in a tellurite microstructured optical fiber pumped at 2 μm," *Optics Express*, vol. 23, no. 4, pp. 4125–4134, 2015.

[11] K. Inoue and H. Toba, "Wavelength conversion experiment using fiber four-wave mixing," *IEEE Photonics Technology Letters*, vol. 4, no. 1, pp. 69–72, 1992.

[12] R. W. Boyd, *Nonlinear Optics, Third Edition.* Academic Press, 3rd ed., 2008.

[13] P. G. Kwiat, K. Mattle, H. Weinfurter, A. Zeilinger, A. V. Sergienko, and Y. Shih, "New high-intensity source of polarization-entangled photon pairs," *Phys. Rev. Lett.*, vol. 75, pp. 4337–4341, Dec 1995.

[14] T. Kim, M. Fiorentino, and F. N. C. Wong, "Phase-stable source of polarization-entangled photons using a polarization sagnac interferometer," *Phys. Rev. A*, vol. 73, p. 012316, Jan 2006.

[15] A. Haase, N. Piro, J. Eschner, and M. W. Mitchell, "Tunable narrowband entangled photon pair source for resonant single-photon single-atom interaction," *Optics letters*, vol. 34, no. 1, pp. 55–57, 2009.

[16] M. Karpiński, M. Jachura, L. J. Wright, and B. J. Smith, “Bandwidth manipulation of quantum light by an electro-optic time lens,” *Nature Photonics*, vol. 11, pp. 53 EP –, 11 2016.

[17] J. Persson, T. Aichele, V. Zwiller, L. Samuelson, and O. Benson, “Three-photon cascade from single self-assembled inp quantum dots,” *Physical Review B*, vol. 69, no. 23, p. 233314, 2004.

[18] T. E. Keller, M. H. Rubin, Y. Shih, and L.-A. Wu, “Theory of the three-photon entangled state,” *Physical Review A*, vol. 57, no. 3, p. 2076, 1998.

[19] J. Douady and B. Boulanger, “Experimental demonstration of a pure third-order optical parametric downconversion process,” *Optics letters*, vol. 29, no. 23, pp. 2794–2796, 2004.

[20] M. Corona, K. Garay-Palmett, and A. B. U’Ren, “Third-order spontaneous parametric down-conversion in thin optical fibers as a photon-triplet source,” *Phys. Rev. A*, vol. 84, p. 033823, Sep 2011.

[21] H. Hübel, D. R. Hamel, A. Fedrizzi, S. Ramelow, K. J. Resch, and T. Jennewein, “Direct generation of photon triplets using cascaded photon-pair sources,” *Nature*, vol. 466, no. 7306, p. 601, 2010.

[22] A. N. Utama, “Elongated cloud of cold 87rb atoms: Towards a brighter source of narrowband photon pairs,” 2016.

[23] D. A. Steck, “Rubidium 87 d line data (2001),” *URL http://steck.us/alkalidata*, vol. 83, 2016.

[24] J. Prodan, A. Migdall, W. D. Phillips, I. So, H. Metcalf, and J. Dalibard, “Stopping atoms with laser light,” *Physical review letters*, vol. 54, no. 10, p. 992, 1985.

[25] B. L. Ng, “Non-linear optics in cold atomic ensemble,” 2017.

[26] C. Foot, “Atomic physics, oxford master series in atomic, optical and laser physics,” 2003.